A numerical study of the influence of hydrogen addition on soot formation in a laminar counterflow ethylene/oxygen/nitrogen diffusion flame

Guo, H.; Liu, Fengshan; Smallwood, Gregory

National Research Council Canada   Conseil national de recherches Canada

Canada

IMECE2004-59407

A NUMERICAL STUDY OF THE INFLUENCE OF HYDROGEN ADDITION ON SOOT FORMATION IN A LAMINAR COUNTERFLOW ETHYLENE/OXYGEN/NITROGEN DIFFUSION FLAME

Hongsheng Guo, Fengshan Liu, and Gregory J. Smallwood
Combustion Research Group
National Research Council Canada
1200 Montreal Road, Ottawa, Ontario, Canada K1A 0R6

ABSTRACT

The influence of hydrogen addition to the fuel on soot formation in an ethylene/oxygen/nitrogen diffusion flame was numerically studied by simulation of three counterflow laminar diffusion flames at atmosphere pressure. The fuel mixtures for the three flames are pure ethylene, ethylene/hydrogen and ethylene/helium, respectively, while the oxidant is a mixture of oxygen and nitrogen. A detailed gas phase reaction mechanism including species up to benzene and complex thermal and transport properties were used. The soot inception and surface growth rates were, respectively, calculated based on benzene and HACA (H-abstraction and C_2H_2-addition) mechanisms.

The predicted results for the three flames were compared and analyzed. It is indicated that although the addition of either hydrogen or helium to the fuel can reduce the soot volume fraction, the addition of hydrogen is more efficient. While the addition of helium reduces soot formation only through dilution, the addition of hydrogen suppresses soot formation through both dilution and chemical reaction effects. This conclusion is qualitatively consistent with available experiments. The simulations revel that the chemically inhibiting effect is caused by the decrease of hydrogen atom concentration in soot formation region, due to the displacement of the primary reaction zone, when hydrogen is added to the fuel.

1. INTRODUCTION

Arthur [1] first observed the effect of atomic hydrogen concentration on the luminosity of a flame due to carbon. During the thermal decomposition of natural gas, it has been shown that the dilution by hydrogen slows down the formation of carbon black particles [2]. In the experimental study of a coflow methane-air diffusion flame, Tesner et al. [3] noted that soot yield decreases with increasing the hydrogen fraction in methane. Dearden and Long [4] found that the addition of hydrogen to fuel results in reduction in sooting rates for ethylene or propane diffusion flame on a Wolfhard-Parker burner. Du et al. [5] observed that hydrogen addition to fuel

results in a substantial decrease in the soot particle inception limit for ethylene, propane and butane counterflow diffusion flames. These investigations demonstrated that the addition of hydrogen to fuel in diffusion flames results in an overall suppression of soot formation. In their experimental study of coflow laminar diffusion flames, Gülder et al. [6] indicated that for an ethylene/air diffusion flame, the addition of hydrogen to fuel suppresses soot formation through both dilution and chemistry effects.

In this paper, the influence of hydrogen addition to the fuel in a counterflow ethylene/oxygen/nitrogen diffusion flame was investigated by numerical simulation. The objective is to use the details from the simulation to gain further insight into those phenomena that have been observed experimentally, especially the chemically inhibiting effect of hydrogen on soot formation. A detailed gas phase reaction mechanism and complex thermal and transport properties were used. For the soot kinetics process, a modified two-equation soot model [7] was used. To identify the relative influences of dilution and direct chemical reaction, the simulations were conducted for three flames, with the fuel mixtures being pure ethylene, ethylene/helium and ethylene/hydrogen, respectively.

2. NUMERICAL MODEL

2.1. Gas Phase Governing Equations

The flame configuration studied in this paper is a counterflow, axi-symmetric laminar diffusion flame. By assuming the stagnation point flow approximation [8], the governing equations for the gas phase are written as

$$\frac{\partial \rho}{\partial t} + \frac{\partial V}{\partial x} = -2\rho G \tag{1}$$

$$L(G) = \frac{\partial}{\partial x}\left(\mu \frac{\partial G}{\partial x}\right) - \rho G^2 + \rho\left(\frac{\partial a}{\partial t} + a^2\right) \tag{2}$$

$$C_p L(T) = \frac{\partial}{\partial x}\left(\lambda \frac{\partial T}{\partial x}\right) - \sum_{k=1}^{KK+1} \rho Y_k V_k C_{pk} \frac{\partial T}{\partial x}$$

$$- \sum_{k=1}^{KK+1} h_k \omega_k M_k + q_r \tag{3}$$

$$L(Y_k) = -\frac{\partial}{\partial x}\left(\rho Y_k V_k\right) + \omega_k M_k \tag{4}$$

where $L(\phi) = \rho \frac{\partial \phi}{\partial t} + V\left(\frac{\partial \phi}{\partial x}\right)$; t is the time; x is the axial coordinate; V is the axial mass flow rate and a is the stretch rate. Quantity G is a combined function of the stretch rate and the stream function; ρ is the density of the mixture; T the temperature; Y_k the mass fraction of the kth gas species; μ the viscosity of the mixture; C_{pk} the constant pressure heat capacity of the kth gas species; M_k the molecular mass of the kth gas species; h_k, V_k and ω_k are, respectively, the species enthalpy, the diffusion velocity and the molar production rate of the kth gas species; and KK is the total gas species number. The production rates of gas species include the contribution due to the soot inception, surface growth and oxidation. The quantities with subscript $KK+1$ correspond to those of soot.

The last term on the right hand side of Eq. 3, q_r, is the radiation heat loss. Our previous investigation [9] showed that the radiation reabsorption is negligible in counterflow ethylene/oxygen/nitrogen diffusion flames. For the sake of simplification, the radiation heat loss due to CO_2, H_2O, CO and soot was calculated by the following optically thin model in the present study:

$$q_r = -4\sigma K_p(T^4 - T_\infty^4) - C f_v T^5 \tag{5}$$

$$K_p = p \sum X_i K_{pi} \tag{6}$$

where σ is the Stefan-Boltzmann constant and K_p is the Plank mean absorption coefficient of the mixture. T_∞ and P respectively denote the environmental temperature (300 K was used in this paper) and pressure. K_{pi} and X_i are the Plank mean absorption coefficient and mole fraction of the ith emitting gas species (which is CO_2, H_2O or CO). The Plank mean absorption coefficients of the emitting gas species were obtained by fitting the data given by Tien [10]. Quantity f_v is the soot volume fraction, and C is a constant being 3.334E-10 (giving a power density in watts/cc for T in Kelvin) [11].

The diffusion velocity (V_k) is written as:

$$V_k = V_{ok} + V_{Tk} + V_c , \qquad k = 1,2,\ldots,KK \tag{7}$$

where V_{ok} and V_{Tk} are the ordinary and thermal diffusion velocities, respectively, for the kth gas species. The ordinary diffusion velocity was calculated by the multi-component formulation [12]. In the present paper, only the thermal diffusion velocities of H_2 and H were considered by the method based on the thermal diffusion ratio [12], while those of all other species were set as zero. The correction diffusion velocity V_c was used to ensure that the net diffusive flux of all gas species and soot is zero. The system of equations, Eqs. 1 – 4,

was closed by the ideal gas state equation and boundary conditions at the fuel and oxidizer jets.

2.2. Soot Model

The relatively detailed soot kinetic models, such as those by Frenklach et al. [13,14], are highly complex and computationally expensive. Conversely, the applicability of purely empirical soot models is questionable under conditions different from those under which they were originally formulated. Based on some semi-empirical assumptions, the simplified two-equation soot model developed by Leung et al. [7] and Fairwhether et al. [15] has been successfully used in our previous studies [16,17] for the simulations of two-dimensional ethylene/air diffusion flames. This two-equation model was also used in the present paper, with the modifications of the soot inception and surface reaction sub-models.

Two transport equations were solved for soot mass fraction and number density, respectively. They are

$$\rho \frac{\partial Y_s}{\partial t} + V \frac{\partial Y_s}{\partial x} = -\frac{\partial}{\partial x}\left(\rho V_{T,s} Y_s\right) + S_m \tag{8}$$

$$\rho \frac{\partial N}{\partial t} + V \frac{\partial N}{\partial x} = -\frac{\partial}{\partial x}\left(\rho V_{T,s} N\right) + S_N \tag{9}$$

where Y_s is the soot mass fraction, N is the soot number density defined as the particle number per unit mass of mixture. Quantity $V_{T,s}$ is the particle thermophoretic velocity. It was obtained by the expression [18]:

$$V_{T,s} = -0.54 \frac{\mu}{\rho T} \frac{\partial T}{\partial x} \tag{10}$$

The source term S_m in Eq. 8 accounts for the contributions of soot nucleation (ω_n), surface growth (ω_g) and oxidation (ω_o). Therefore

$$S_m = \omega_n + \omega_g - \omega_o \tag{11}$$

The soot nucleation is calculated by the model described by Beltrame et al. [19]. It assumed the following reaction:

$$C_6H_6 + C_6H_5 \Rightarrow 12C(S) + 5H_2 + H \qquad \text{R1}$$
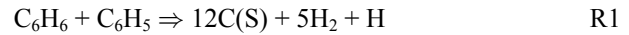
where C(S) represents the carbon atoms in soot. The advantage of this approach over the acetylene based model used in our previous studies [16,17] is the possibility of predicting soot inception based on PAH-PAH reactions without substantially affecting the computational time. The introduction of phenyl (C_6H_5) into the inception step is because it plays a key role in the formation of large PAH. More details of this nucleation model can be found from [19]. The soot nucleation rate is thus calculated as

$$\omega_n = 12 M_s k_n [C_6 H_6][C_6 H_5] \tag{12}$$

where M_s is the molar mass of soot (12.011 g/mole), $[C_6H_6]$ and $[C_6H_5]$ are the mole concentrations of benzene and phenyl, respectively, (mole/cm^3), and $k_n = 5.0E+13\exp\left(-21000/T\right)$.

The soot surface growth and oxidation were assumed to follow the H-abstraction and C_2H_2-addition (HACA) reaction sequence given by Appel et al. [20]. The rates of surface growth and soot oxidation (ω_g and ω_o) were calculated based on the kinetics data of table 3 in Ref. [20]. The only modification is the parameter α, the fraction of the reactive surface available for chemical reactions, since a different soot particle dynamics model from that in [20] was employed. A constant value of 0.06 for α was found to fit the available experimental data well in this study.

The source term S_N in Eq. 9 accounts for the soot nucleation and agglomeration, and was calculated as [7, 15]:

$$S_N = \frac{\omega_n}{M_s C_{\min}} N_A -$$
$$2C_a \left(\frac{6M_S}{\pi\rho_{C(S)}}\right)^{1/6} \left(\frac{6\kappa T}{\rho_{C(S)}}\right)^{1/2} \left[C(s)\right]^{1/6}\left[\rho N\right]^{11/6} \qquad (13)$$

where N_A is Avogadro's number (6.022 x 10^{23} particles/mole), C_{min} is the number of carbon atoms in the incipient carbon particle (100) [7], κ is the Boltzmann constant (1.38x10^{-16} erg/K), $\rho_{C(S)}$ is the soot density (1.9 g/cm^3), [C(s)] is the mole concentration of soot (mole/cm^3), and C_a is the agglomeration rate constant for which a value of 6.0 was used.

2.3. Numerical Methods

The calculations were carried out with a code revised from that of Kee et al. [21]. Upwind and center difference schemes were respectively used for the convective and diffusion terms in all the governing equations. Adaptive refinement of meshes was done. The pressure and environment temperature were, respectively, 1 atm and 300 K. The distance between the two opposed nozzles was 1.5 cm for all the calculations.

The chemical reaction mechanism adopted is a combination of GRI-Mech 3.0 [22] and a reaction sequence leading to the formation of benzene. The C1-C2 chemistry is essentially the GRI-Mech 3.0 with the removal of the reactions and species related to NO$_x$ formation (except N$_2$). The reactions leading to the formation of benzene are those in table 1 of [19]. This reaction mechanism includes 48 gas species and 300 reactions.

3. RESULTS AND DISCUSSION

The numerical model was used to investigate the effect of hydrogen addition on soot formation in a laminar counterflow ethylene/oxygen/nitrogen diffusion flame. To validate the soot model, two laminar counterflow ethylene/oxygen/nitrogen diffusion flames experimentally studied by Hwang et al. [23] were calculated first, with the fuel for these two flames being pure ethylene (C$_2$H$_4$) and the oxidants being (24%O$_2$ + 76%N$_2$) and (28%O$_2$ + 72%N$_2$), respectively. The stretch rate of both flames is the same as 27.5 1/s. This stretch rate was selected to match the global velocity gradient in the experiments [23].

The calculated soot volume fractions for the two flames are compared with the experimental data of [23] in Fig. 1. The fuel and oxidant nozzles are respectively on the right and left sides. It is observed that there is some quantitative difference between the simulations and experiments. For both flames, the peak soot volume fractions are a little underpredicted, and the calculated positions of peak soot volume fraction are slightly shifted to the fuel side. However, the simulation captured the general feature of soot in the flames. The basic soot volume fraction distributions agree well with experiments, and the increase of soot volume fraction with the rise of oxygen concentration in the oxidant was predicted. Therefore the soot model used is reasonable.
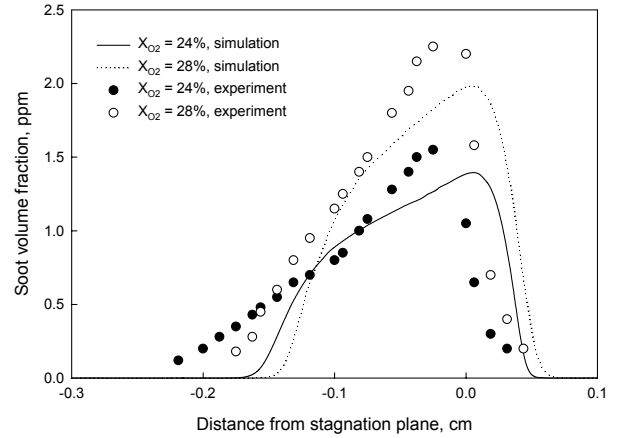

Fig. 1 Predicted and measured [23] soot volume fractions of two ethylene/oxygen/nitrogen diffusion flames. X$_{O2}$ represents the volume fraction of oxygen in oxidant stream.
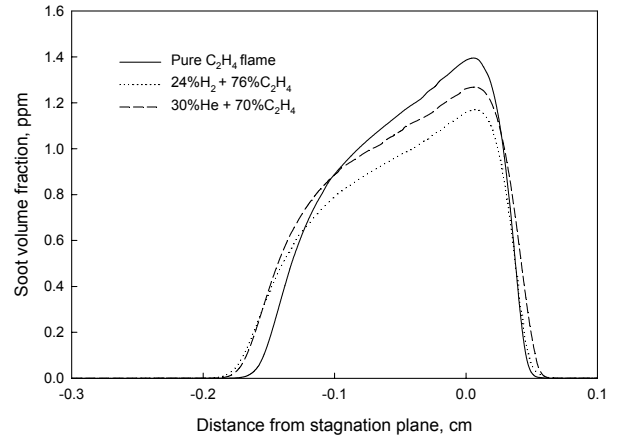

Fig. 2 Predicted soot volume fractions for three flames.

Now we investigate the effect of hydrogen addition on soot formation in ethylene diffusion flame. The base flame is the first ethylene/oxygen/nitrogen diffusion flame discussed above, with the fuel being pure ethylene and oxidant being (24%O$_2$ + 76%N$_2$). To study the effect of hydrogen addition, two diluted ethylene/oxygen/nitrogen diffusion flames were also simulated. The fuel streams for the two diluted flames are, respectively, (30%He + 70%C$_2$H$_4$) and (24%H$_2$ + 76%C$_2$H$_4$), while the oxidant stream of them is the same as the base flame, i.e. (24%O$_2$ + 76%N$_2$). The selection of 24% hydrogen and 30% helium in the two diluted flames is to match the experimental condition in [6].
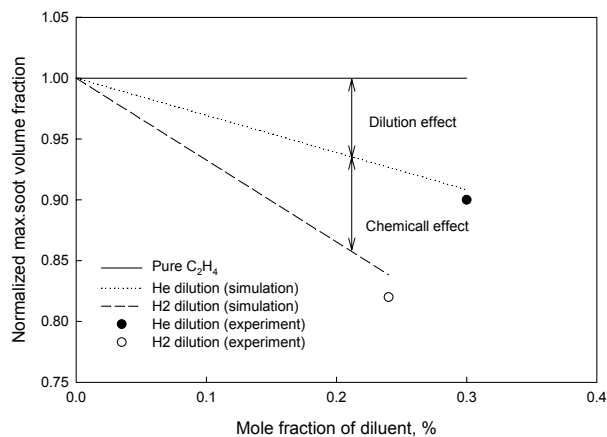
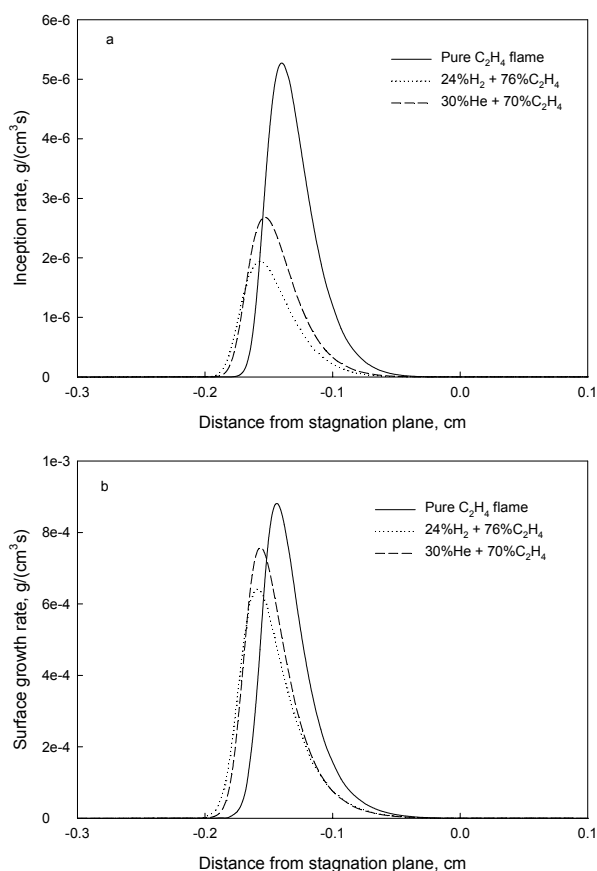Fig. 3 Predicted and measured [6] normalized maximum soot volume fraction.

Fig. 4 Inception and surface growth rates.

Figure 2 shows the predicted soot volume fractions for the three (the base and the two diluted) flames. It is revealed that the addition of either hydrogen or helium to the fuel reduces soot volume fraction in the flame. Although the fraction of hydrogen (24%) added to the fuel is lower than that of helium (30%), the soot volume fraction reduction due to hydrogen addition is more significant.

The change of the normalized maximum soot volume fraction, defined as the ratio of the maximum soot volume

fraction in the diluted flames to that in the undiluted (base) flame, with hydrogen and helium addition into ethylene is shown in Fig. 3. For comparison, the experimental data [6] from two-dimensional axi-symmetric ethylene/air diffusion flames are also shown. As illustrated, although counterflow flame configuration was used in this study, the basic feature of the hydrogen addition effect observed experimentally by Gülder et al. [6] was captured.

Since the studied ethylene/oxygen/nitrogen diffusion flame is a soot formation (SF) flame and the soot oxidation is negligible [23], the analysis below will focus on the soot inception and surface growth processes. The inception and surface growth rates for the three flames are shown in Fig. 4. It is indicated that the addition of hydrogen or helium to the fuel reduces both inception and surface growth rates in the ethylene/oxygen/nitrogen diffusion flame. However the addition of hydrogen is more efficient to suppress the formation of soot.

When hydrogen or helium is added to the fuel, they may affect soot formation through the effects of thermal, dilution and direct chemical reaction. Since both hydrogen and helium are transparent in terms of radiation heat transfer and their specific heats are smaller than that of ethylene, there is no thermal effect that can cause the reduction in soot formation rate when they are added to ethylene.

Helium is an inert species, so the reduction of soot formation due to its addition to ethylene must be the result of dilution.

Hydrogen has similar specific heat and transport properties to helium, and, as a fuel, a similar adiabatic flame temperature to ethylene. Its dilution effect on soot formation should be similar to that of helium. Therefore the difference in soot volume fraction between the helium and hydrogen diluted flames should be the result of the chemically inhibiting effect of hydrogen. This direct chemical effect causes the addition of hydrogen to the fuel more efficient than that of helium at suppressing soot yields in ethylene diffusion flames. We shall analyze the chemically inhibiting effect of hydrogen addition by comparing the soot characteristics in the hydrogen and helium diluted flames.

First we will examine the effect of hydrogen addition on soot inception. From the inception model (Eq. 12), we know that the soot inception rate depends on temperature and the concentrations of benzene (C_6H_6) and phenyl (C_6H_5). Figure 5 illustrates the temperatures for the three flames (pure ethylene flame and the hydrogen and helium diluted flames). It is demonstrated that although the peak temperature of the hydrogen diluted flame is higher than that of the helium diluted flame, the difference between the two flames is negligible in the inception and surface growth region (-0.2 to - 0.1 cm). This is because the primary reaction zone is shifted to the oxidant (left) side for the hydrogen diluted flame, due to the higher mass diffusivity of hydrogen. Therefore temperature is not the significant factor causing the lower inception and surface growth rates for the hydrogen diluted flame.

Figure 6 depicts the mole fractions of C_6H_6 and C_6H_5 in the three flames. It is observed that the concentration of C_6H_6 in the hydrogen diluted flame is higher than that in the helium diluted flame in the inception region, while the situation reverses for the concentration of C_6H_5. Consequently the lower

concentration of C_6H_5 in the inception region is the factor causing the lower inception rate in the hydrogen diluted flame.
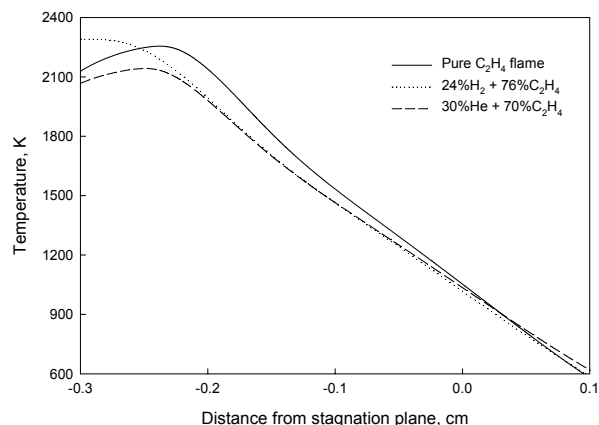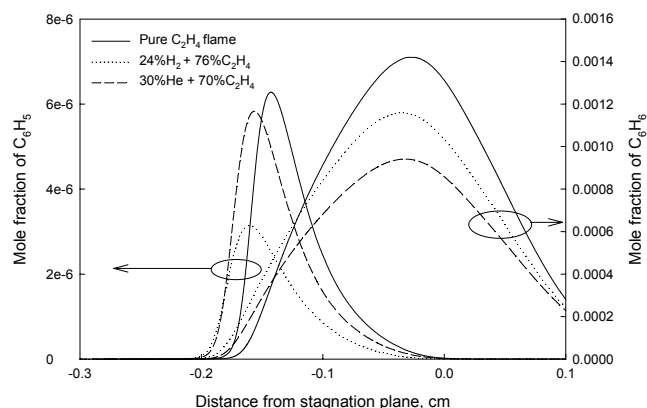

Fig. 5 Temperature distributions.

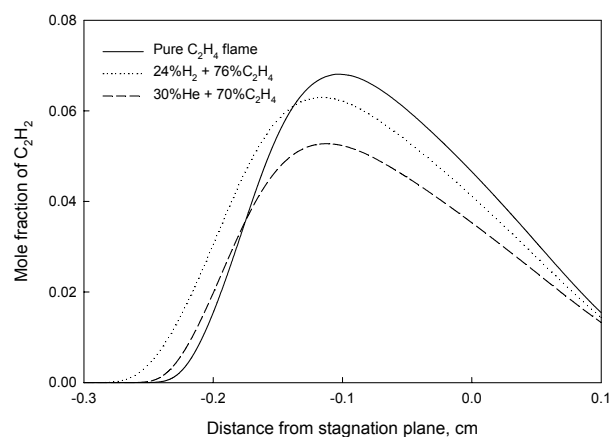Fig. 6 Mole fractions of C_6H_6 and C_6H_5 for the three flames.

Fig. 7 Mole fractions of C_2H_2 in the three flames.

The higher concentration of C_6H_6 in the hydrogen diluted flame results from the higher concentration of acetylene (C_2H_2), as in Fig. 7, since acetylene plays an important role in the formation of C_6H_6. The profiles of the acetylene production rate are shown in Fig. 8. Comparing the production rates of acetylene in the hydrogen and helium diluted flames, it is found
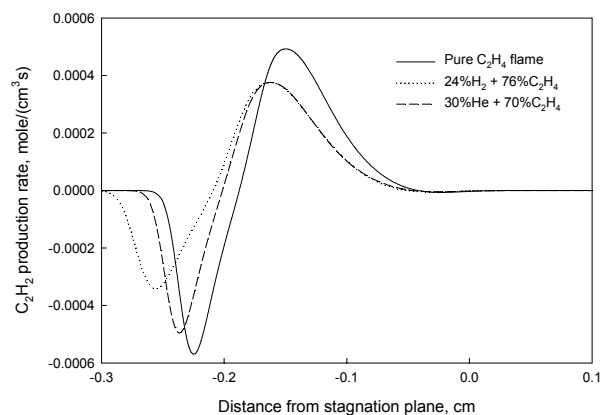

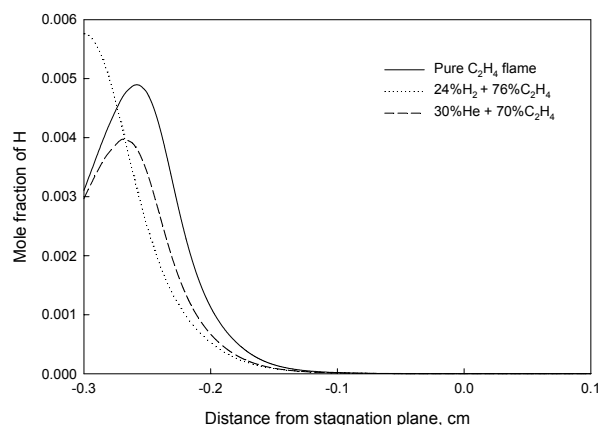Fig. 8 Production rates of acetylene (C_2H_2) in the three flames.

Fig. 9 Mole fractions of H in the three flames.

that the formation rates (positive) of acetylene in the two flames are similar. However the absolute value of the destruction (negative) rate of acetylene in the hydrogen diluted flame is smaller than that in the helium diluted flame. A sensitivity analysis indicates that the most significant formation and destruction reactions of acetylene are $H + C_2H_2$ (+M) = C_2H_3 (+M) and $O + C_2H_2 = H + HCCO$, respectively. Due to the fact that more molecular and atomic oxygen are consumed by hydrogen in the hydrogen diluted flame, the rate of the destruction reaction of acetylene in the hydrogen diluted flame is lower. As a result, the concentration of acetylene in the hydrogen diluted flame is higher, which leads to more benzene.

The most important formation reaction of phenyl (C_6H_5) is $C_6H_6 + H = C_6H_5 + H_2$. Since there is negligible difference in temperatures between the hydrogen and helium diluted flames and the concentration of C_6H_6 in hydrogen diluted flame is higher, the factor causing the lower C_6H_5 concentration in the hydrogen diluted flame should be the lower concentration of H. Figure 9 gives the profiles of H in the three flames. It is found that although in the hydrogen diluted flame, the peak concentration of H is higher, the concentration of H in the inception and growth region is lower. Similar to the profiles of temperature in Fig. 5, this is a result of the higher mass diffusivity of hydrogen, which causes the primary reaction zone to shift to the oxidant side (left) for the hydrogen diluted flame. It is the lower concentration of H in the inception region that

causes the lower C_6H_5 concentration, which leads to the lower soot inception rate in the hydrogen diluted flame than in the helium diluted flame.
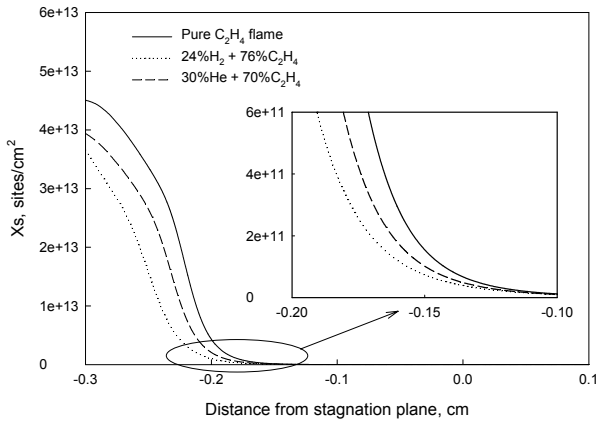

Fig. 10 Number density of surface sites.

It should be pointed out that the above discussion of hydrogen addition effect on the inception rate of soot is based on the inception model used in this study. In reality, soot particle may not be directly formed from benzene, but from some larger size PAH. However as indicated by Frenklach et al. [14], the growth of aromatic rings from the first ring to larger size PAH is mainly through the H-abstraction and C_2H_2-addition reaction sequence, and thus H plays an important role in the growth of aromatic rings. Although the PAH growth chemistry beyond benzene (C_6H_6, the first aromatic ring) was not included in this study, the introduction of phenyl (C_6H_5) to the soot inception model to certain extent accounts for the effect of H-abstraction on soot inception. From this viewpoint, we can say that the current simplified soot inception model is reasonable. Therefore we can conclude that it is the lower concentration of H in the inception region causes the lower inception rate in the hydrogen diluted flame than that in the helium diluted flame.

We now examine the surface growth. Based on the HACA reaction sequence, the soot surface growth rate equals $k_{C2H2}[C_2H_2]\alpha\chi_s A_s / N_A$, where k_{C2H2} is the per-site rate coefficient for C_2H_2-addition, $[C_2H_2]$ is the mole concentration of acetylene, α is the fraction of reactive surface available for surface reactions, A_S is the particle surface area, N_A is Avogadro's number, and χ_S is the number density of surface sites for C_2H_2-addition. It is seen that the factors affecting surface growth rate include the acetylene addition rate per site ($k_{C2H2}[C_2H_2]$), the particle surface area (A_S), and the number density of surface sites (χ_S). As we have indicated above, the difference in temperature between the hydrogen and helium diluted flames is negligible in soot formation region, and the concentration of acetylene in the hydrogen diluted flame is higher than that in the helium diluted flame. Therefore compared to the addition of helium, the addition of hydrogen tends to increase the C_2H_2-addition rate per site.

As for the second factor affecting surface growth rate, the addition of hydrogen more efficiently reduces the soot inception rate and thus the particle surface area than that of helium, as discussed before. This causes the surface growth rate

to decrease more significantly in the hydrogen diluted flame than in the helium diluted flame.

In addition, the number density of surface sites (χ_S), obtained by assuming steady state, in the hydrogen diluted flame is also lower than that in the helium diluted flame, as shown in Fig. 10. The two key reactions in the HACA reaction sequence are: C_{soot}-H + H = $C_{soot}\cdot$ + H_2 and $C_{soot}\cdot$ + $C_2H_2 \Rightarrow C_{soot}$-H + H. The former is the H-abstraction reaction to form the active site for the C_2H_2-addition, and latter is the C_2H_2-addition reaction. The H-abstraction reaction is reversible, but the calculation indicates that the rate of the reverse reaction is much smaller than that of the forward reaction. Since the temperature difference is negligible between the hydrogen and helium diluted flames, the lower H concentration in the growth region of hydrogen diluted flame, as in Fig. 9, leads to the lower H-abstraction rate. Consequently the number density of surface sites for C_2H_2-addition in the hydrogen diluted flame is lower than that in the helium diluted flame. This is another factor leading to the lower surface growth rate in the hydrogen diluted flame than that in the helium diluted flame.

Both the smaller soot particle number density due to the lower inception rate and the smaller number density of surface sites for C_2H_2-addition result in the lower surface growth rate in the hydrogen diluted flame than in the helium diluted flame.

Therefore we can conclude that the addition of hydrogen to ethylene is more efficient than that of helium at suppressing soot formation in counterflow ethylene/oxygen/nitrogen diffusion flame. It is because the addition of helium suppresses soot formation only through the dilution effect, while the addition of hydrogen suppresses soot formation through both dilution and chemical effects. The chemically inhibiting effect of hydrogen addition on soot formation is because the concentration of H is reduced in the soot inception and surface growth regions, and thus the rate of H-abstraction reaction of both PAH growth and surface growth is reduced. The reduction of H concentration in the inception and surface growth region is caused by the shift of the primary reaction zone to the oxidant side, when hydrogen is added to the fuel. The agreement of the predicted soot formation and the available experiment data by Gülder et al. [6] further supports the viewpoint that HACA reaction sequence plays an important role in soot inception and surface growth processes.

4. CONCLUSIONS

The influences of hydrogen and helium addition to fuel on soot formation have been numerically studied by the simulations of counteflow ethylene/oxygen/nitrogen diffusion flames at atmospheric pressure. The results indicate that although the addition of both hydrogen and helium to ethylene can reduce the soot formation rates, the addition of hydrogen is more efficient. The addition of helium reduces the soot formation only through dilution, while the addition of hydrogen suppresses the soot formation through both dilution and direct chemical reaction. This conclusion is consistent with the available experiments. The chemical effect is caused by the decrease of the hydrogen atom concentration in soot inception and surface growth regions due to the displacement of the primary reaction zone, when hydrogen is added to ethylene.

6   Copyright © 2004 by ASME

REFERENCES

1. Arthur, J. R., 1950, "Some Reactions of Atomic Hydrogen in Flames", *Nature,* 165, pp.557-558.
2. Tesner, P.A., 1958, "Formation of Dispersed Carbon by Thermal Decomposition of Hydrocarbons", *Seventh Symposium (Int.) on Combustion*, The Combustion Institute, pp.546-553.
3. Tesner, P. A., Robinovitch, H. J., and Rafalkes, I.S*.,* 1960*,* "The Formation of Dispersed Carbon in Hydrocarbon Diffusion Flames", *Eighth Symposium (Int.) on Combustion*, The Combustion Institute, pp.801-806.
4. Dearden, P., and Long, R., 1968, "Soot Formation in Ethylene and Propane Diffusion Flames". *J. Appl. Chem.*, 18, pp.243-251.
5. Du, D.X., Axelbaum, R.L., and Law, C.K., 1995, "Soot Formation in Strained Diffusion Flames with Gaseous Additives", *Combust. Flame,* 102, pp.11-20.
6. Gülder, Ö.L., Snelling, D.R., and Sawchuk, R.A*.,* 1996, "Influence of Hydrogen Addition to Fuel on Temperature Field and Soot Formation in Diffusion Flames", *Twenty-Sixth Symposium (Int.) on Combustion*, The Combustion Institute, pp.2351-2358.
7. Leung, K.M., Lindstedt, R.P. and Jones, W.P., 1991, "A Simplified Reaction Mechanism for Soot Formation in Nonpremixed Flames", *Combust. Flame,* 87, pp.289-305.
8. Giovangigli, V., and Smooke, M.D., 1987, "Extinction of Strained Premixed Laminar Flames with Complex Chemistry", *Combust. Sci. Tech*., 53, pp.23-49.
9. Liu, F., Guo, H., Smallwood, G.J., and Hafi, M.E., 2004, "Effects of Gas and Soot Radiation on Soot Formation in Counterflow Ethylene Diffusion Flames", J. *Quantitative Spectroscopy & Radiative Transfer,* 84, pp.501-511.
10. Tien, C.L., 1967, "Thermal Radiation Properties of Gases", *Advances in Heat Transfer,* 5, pp.253-324.
11. Smooke, M.D., Mcenally, C.S., Pfefferle, L.D., Hall, R.J., and Colket, M.B., 1999, "Computational and Experimental Study of Soot Formation in a Coflow, Laminar Diffusion Flame", *Combust. Flame,* 117, pp.117-139.
12. Kee., R.J., Dixon-Lewis, G., Warnatz, J., Coltrin, M.E., and Miller, J.A., 1986, "A Fortran Computer Code Package for the Evaluation of Gas-Phase, Multicomponent Transport Properties", Sandia Report, SAND 86-8246.
13. Frenklach, M. and Wang, H., 1990, "Detailed Modeling of Soot Particle Nucleation and Growth", *Twenty-Third Symposium (Int.) on Combustion*, The Combustion Institute, pp.1559-1566.
14. Frenklach, M., and Wang, H., 1994, "Detailed Mechanism and Modeling of Soot Particle Formation", *Soot Formation in Combustion: Mechanisms and Models (Bockhorn, H. Ed.),* Springer Series in Chemical Physics, 59, Springer-Verlag, Berlin, pp. 164-190.
15. Fairwhether, M., Jones, W.P. and Lindstedt, R.P., 1992, "Predictions of Radiative Transfer from a Turbulent Reacting Jet in a Cross-Wind", *Combust. Flame,* 89, pp.45-63.
16. Guo, H., Liu, F., Smallwood, G.J., and Gülder, Ö.L., 2002, "The Flame Preheating Effect on Numerical Modelling of Soot Formation in a Two-Dimensional Laminar Ethylene-Air Diffusion Flame", *Combust. Theory Modelling,* 6, pp.173-187.
17. Guo, H., Liu, F., Smallwood, G.J., and Gülder, Ö.L., 2002, "A Numerical Study of the Influence of Transport Properties of Inert Diluents on Soot Formation in a Coflow Laminar Ethylene-Air Diffusion Flame", *Proc. Comb. Inst*., 29, pp.2359-2365.
18. Talbot, L., Cheng, R.K., Schefer, R.W., and Willis, D.R., 1980, "Thermophoresis of Particles in a Heated Boundary Layer", *J. Fluids Mech*., 101, pp.737-758.
19. Beltrame, A., Porshnev, P., Merchan-Merchan, W., Saveliev, A., Fridman, A., Kennedy, L.A., Petrova, O., Zhdanok, S., Amouri, F., and Charon, O., 2001, "Soot and NO Formation in Methane-Oxygen Enriched Diffusion Flames", *Combust. Flame,* 124, pp.295-310.
20. Appel, J., Bockhorn, H., and Frenklach, M., 2000, "Kinetic Modeling of Soot Formation with Detailed Chemistry and Physics: Laminar Premixed Flames of C2 Hydrocarbons", *Combust. Flame,* 121, pp.122-136.
21. Kee, R.J., Grcar, J.F., Smooke, M.D., and Miller, J.A., 1985, "A Fortran Program for Modeling Steady Laminar One-Dimensional Premixed Flames", Sandia Report, SAND85-8240.
22. Smith, G.P., Golden, D.M., Frenklach, M., Moriarty, N.W., Eiteneer, B., Goldenberg, M., Bowman, C.T., Hanson, R.K., Song, S., Gardiner, W.C., Jr., Lissianski, V.V., and Qin, Z., http://www.me.berkeley.edu/gri_mech/.
23. Hwang, J.Y., and Chung, S.H., 2001, "Growth of Soot Particles in Counterflow Diffusion Flames of Ethylene", *Combust. Flame,* 125, pp.752-762.